Rearrangement Pathways of Arylperoxy Radicals. I. The Azabenzenes

Michael J. Fadden and Christopher M. Hadad*

Department of Chemistry, 100 West 18th Avenue, The Ohio State University, Columbus, Ohio 43210

Received: March 3, 2000; In Final Form: April 26, 2000

The potential energy surfaces for the reaction of pyridinyl radicals with O_2 have been studied using the B3LYP method. The initial production of the pyridinylperoxy radical followed by either simple decomposition or rearrangement to yield the intermediates (pyridinyloxy, dioxiranylpyridinyl, or dioxetanylpyridinyl radicals) has been explored. Transition-state structures for most of the steps are presented as well as relative free energies over a range of temperatures from 298 to 2000 K. The energetics of the analogous intermediates for the reaction of O_2 and other azabenzene radicals derived from pyridazine, pyrimidine, and pyrazine are also provided. O_2 dissociation from the arylperoxy radical is preferred rather than the loss of O atom to generate the corresponding aryloxy radical, and this preference is contrary to phenylperoxy radical decomposition. However, the formation of a dioxiranyl radical intermediate is the most accessible intermediate from the peroxy precursor at temperatures $\leq$500 K. Dioxetanyl intermediates are less favored but may provide a route to NO_x generation from nitrogen substitution in aromatic fuels.

I. Introduction

Understanding the processes involved in coal combustion is difficult owing to the complex nature of coal and the diverse structural units present in the different ranks of coal.[1] To resolve the chemical processes that occur during coal combustion, many workers have relied on the use of monocyclic model compounds, such as benzene, pyridine, furan, and thiophene, to gain some understanding into the combustion of organic fuels. As the "standard" aromatic ring, numerous studies have been completed on the oxidative, thermal decomposition of benzene.[2−6]

Nitrogen-containing aromatic rings also constitute a significant fraction of coal, and oxidation of these units contribute to NO_x generation in coal-fired boilers.[7] Most studies with pyridine or the diazines have focused on the pyrolysis[8−10] of these compounds, and oxidative pyrolysis has been less well studied.[11] C−H bond dissociation enthalpies (BDEs) have been determined for some of these monocyclic azabenzenes, and a significant stabilizing effect on the radical has been noted when nitrogen is present in the ring.[12]

Several studies on the reaction of phenyl radical (**1**) with O_2 have shown the importance of phenylperoxy radical (**2**) as a key intermediate.[13,14] As depicted in Figure 1, the phenylperoxy radical can then further decompose or rearrange via a number of different pathways, including a phenoxy radical (**3**), a dioxiranyl radical (**4**), or possibly a dioxetanyl radical (**5**) before ultimately decomposing to the cyclopentadienyl radical, CO, CO_2, and a number of other hydrocarbons.[6,15,16]

Recently, we have explored the mechanisms for the reaction of phenyl radical with O_2 in great detail (including transition states), and earlier, we have presented a thermodynamic study for the decomposition of some other aryl species, including the 2-pyridinyl radical.[15] We, and others, have shown that density functional theory (DFT) methods[17] can be accurately applied to aromatic radicals, and at reasonable expense, as spin contamination is not a significant problem.[12,18]

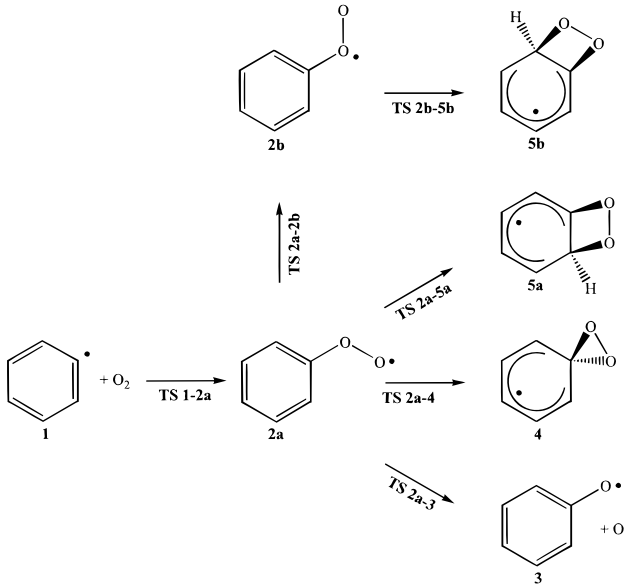

Figure 1. Reaction mechanism of phenyl radical with O_2. This numbering sequence will be used throughout the text, tables, and figures to identify the analogous intermediate and transition state for each azabenzene system.

In this paper, we present a detailed potential energy surface for the reaction of pyridinyl radicals with O_2, as we have explored the analogous decomposition pathways as depicted in Figure 1 for phenyl radical with O_2. In particular, the reactivity of the pyridinylperoxy and diazaarylperoxy radicals are compared with phenylperoxy radicals at temperatures ranging from 298 to 2000 K.

II. Computational Methods

All geometry optimizations, vibrational frequency calculations, and single-point energy determinations were completed with Gaussian 94 and 98 at the Ohio Supercomputer Center or on our IBM RS/6000 workstations.[19,20]

* Corresponding author: hadad.1@osu.edu, 614-292-1685 (FAX).

10.1021/jp0008492 CCC: $19.00
Published on Web 06/03/2000

The B3LYP/6-31G* hybrid density functional theory level was employed to determine the optimized geometries and vibrational frequencies of all stationary points.[21−24] Single-point energies were also determined at the B3LYP/6-311+G** level, as it has been shown that there is a small basis set effect with oxygen-containing systems when determining C−H bond dissociation energies.[25] The B3LYP/6-311+G** single-point energies should provide better relative energies. We have also determined single-point energies at the UCCSD(T)/6-31G** level of theory for several key intermediates and transition states in order to compare with our B3LYP results.[26] All basis sets used six Cartesian d functions.

Vibrational frequencies were calculated for each stationary point in order to confirm each structure as a minimum or a saddle point, and each stationary point had the correct number of real and imaginary vibrational frequencies. The zero-point vibrational energy (ZPE) corrections were also obtained and scaled by a factor of 0.9806.[27] All transition states were confirmed to connect to the corresponding reactant and product by displacing (typically 10%) the geometry along the reaction coordinate for the imaginary vibrational frequency in either direction, which was then followed by a careful optimization (opt=calcfc or opt=calcall) to the corresponding minimum.

Spin contamination for most stationary points was negligible. The $\langle S^2 \rangle$ values for all of the minima and for most of the transition states fell below 0.80 for these doublet species. Those specific transition states that suffered from excessive spin contamination will be discussed below, and their energies and geometries are considered to be suspect.

To determine the thermodynamic contribution to the free energy of each molecule at temperatures ranging from 298 to 2000 K, Thermo94[28] was used to calculate the partition function contributions derived from the optimized geometry and the unscaled vibrational frequencies as calculated by Gaussian. The overall Gibbs free energy at each temperature was derived from the single-point energy, the scaled ZPE, the thermodynamic contribution (enthalpy and entropy), and the electronic contribution to the free energy. The only molecule that received different treatment was O atom, where experimentally[29] determined splitting energies were included in the electronic component of the partition function for the free energy calculation.

The energies discussed throughout are Gibbs free energies computed at the B3LYP/6-311+G**//B3LYP/6-31G* level (at 298 K, unless noted otherwise) and are relative to the Gibbs free energy of the corresponding arylperoxy radical.

III. Mechanism of the Pyridinyl Radical + O_2 Reaction

A. Formation of the Pyridinylperoxy Radical Intermediate (1 → 2a). Experimentally, pyridinylperoxy radicals are formed by the rapid addition of O_2 to the pyridinyl radical in the condensed phase.[30] At 298 K, this reaction is calculated to be exoergic by −28.5 kcal/mol for 2-pyridinyl radical, −30.4 kcal/mol for 3-pyridinyl radical, and −29.9 kcal/mol for 4-pyridinyl radical. The free energy of activation ($\Delta G^{\ddagger}$, 298 K) for the formation of 2-pyridinylperoxy and 4-pyridinylperoxy radicals from their respective precursors is 6.2 kcal/mol, while the corresponding value for 3-pyridinylperoxy radical is 7.2 kcal/mol.

The transition states for the formation of the pyridinylperoxy radicals have been found, but they suffer from excessive spin contamination ($\langle S^2 \rangle \sim 1.8$) and have very small imaginary vibrational frequencies, ranging from 7.9*i* to 16.5*i* cm^{-1}. These values are very similar to previously reported calculations for the addition of O_2 to phenyl radical where $\Delta G = -32.3$ kcal/mol and $\Delta G^{\ddagger} = 6.1$ kcal/mol, and the transition state for formation of phenylperoxy radical had $\langle S^2 \rangle = 1.76$ and an imaginary vibrational frequency of 6.2*i* cm^{-1}.[16] The lowest energy conformations of the 2-, 3-, and 4-pyridinylperoxy radicals have C_s symmetry with $^2A''$ electronic ground states.

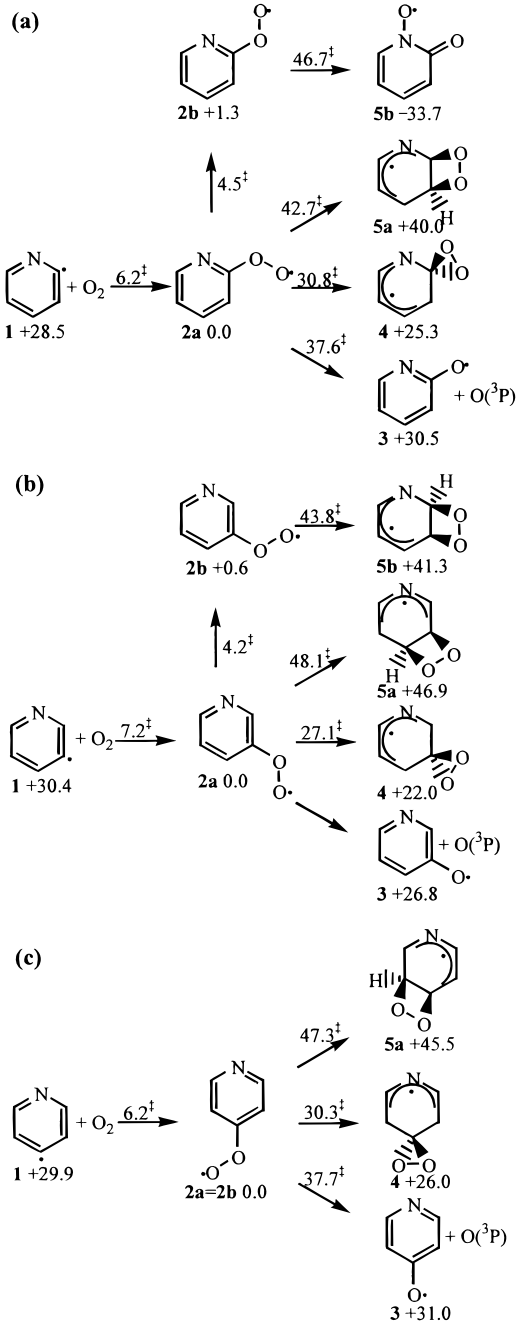

Figure 2. Mechanisms of the (a) 2-pyridinyl + O_2, (b) 3-pyridinyl + O_2 and (c) 4-pyridinyl + O_2 reactions showing Gibbs free energy of activation barriers (relative to the appropriate reactant) and Gibbs free energies of each intermediate at 298 K (relative to the corresponding **2a**) at the B3LYP/6-311+G**//B3LYP/6-31G* level.

The rearrangement or unimolecular decomposition of the pyridinylperoxy radicals to yield several different intermediates was explored. To compare structures between phenyl radical and the azaaryl radicals, we have chosen to use a consistent naming system, as depicted in Figure 1, where, for example, each **2a** isomer is a peroxy radical derived from the corresponding aryl radical. Also, the **a** isomer is always more stable than the **b** isomer when there is more than one unique way to orient

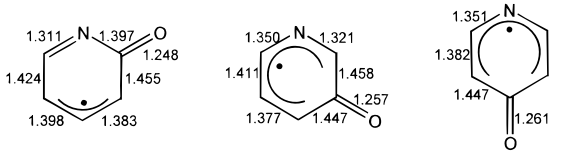

2-pyridinyloxy (**3**) C_s, ^{2}A" 3-pyridinyloxy (**3**) C_s, ^{2}A" 4-pyridinyloxy (**3**) C_s, ^{2}A"

Figure 3. Molecular structures and critical bond lengths (Å) of the pyridinyloxy radicals (B3LYP/6-31G*).

the group. (For phenyl radical, these **a** and **b** isomers are the same structure.)

The first pathway in the unimolecular decomposition of pyridinylperoxy radical (**2a**) is the cleavage of the O−O bond to yield the pyridinyloxy radical and O atom (**2a** → **3**). Another pathway would be the rearrangement of the pyridinylperoxy radical to form a dioxiranyl intermediate (**2a** → **4**). Finally, the production of dioxetanyl intermediates either from the lowest energy conformation of pyridinylperoxy radical (**2a** → **5a**) or from a rotation of the peroxy functional group followed by ring closure (**2a** → **2b** → **5b**) are also possibilities. All of the energies reported in the tables as well as those discussed within the text are relative to the energy of the most stable conformation of the respective arylperoxy radical (i.e., the corresponding **2a** structure).

B. Unimolecular Decomposition of the Pyridinylperoxy Radicals to Yield Pyridinyloxy Radicals and O Atom (2a → 3). Pyridinylperoxy radicals can decompose via the homolysis of the O−O bond to produce the pyridinyloxy radical (**3**, Figure 2) and O atom. This reaction is an endoergic process at 298 K for the 2-, 3-, and 4-pyridinylperoxy radicals. The order of stability of the pyridinyloxy radicals as compared to their peroxy radical precursors is 3- > 2- > 4-pyridinyloxy radical. From the B3LYP/6-31G* optimized geometries of these molecules (Figure 3), it is apparent that all of the pyridinyloxy radicals delocalize the unpaired electron around the ring, resulting in some enhanced stability. This delocalization also occurs for phenoxy radical.[16] The 2-pyridinyloxy radical has dominant C═N and C═C bonds in the ring. The 4-pyridinyloxy radical is more delocalized, and the C−N bonds are more similar to the 3-pyridinyloxy radical. Each of these structures has an azapentadienyl radical delocalization; however, they differ in the location of the N atom relative to the unpaired electron. In the 3-pyridinyloxy radical, the unpaired electron cannot be on N, and this confers some stability as the electron−electron repulsion between the N lone pair (in the σ system) and the unpaired electron (in the π system) is minimized. In the 2- and 4-pyridinyloxy radicals, the unpaired electron can be delocalized onto N. These results are not surprising given that the experimental O−H bond dissociation energies of 2-, 3-, and 4-pyridinol are 99, 93, and 100 kcal/mol, respectively.[31]

The differences in stability of these pyridinyloxy intermediates are reflected in the ΔG(298 K) for the unimolecular decomposition of the pyridinylperoxy radicals to the pyridinyloxy radical and O atom (at infinite separation). The endoergicity of this reaction for 3-pyridinylperoxy radical is +26.8 kcal/mol, which is very similar to the +27.3 kcal/mol value calculated for the analogous reaction with phenylperoxy radical. This energy is 3−4 kcal/mol more favorable than for the 2- or 4-pyridinylperoxy radicals (Table 1).

The free energies of activation for the scission of the O−O bond in 2- and 4-pyridinylperoxy radicals have been determined, but attempts to find the analogous transition state for 3-pyridinylperoxy radical have been fruitless. The $\Delta G^{\ddagger}$(298 K) for the decomposition of 2- and 4-pyridinylperoxy radical is ∼38 kcal/mol with barriers of ∼7 kcal/mol for the reverse reaction. In an analogous computational study, it was determined that the O atom addition to vinyloxy radical (CH_2═CHO•) to form CH_2═$CHOO$• is nearly barrierless.[32] This observation correlates well with the B3LYP/6-311+G**//B3LYP/6-31G* bottom-of-the-well energy difference of only ∼0.1 kcal/mol between the 2- and 4-pyridinyloxy radicals and O atom complexes, as compared to their respective transition states that lead to the peroxy radicals. Also, both calculated transition states suffer from excessive spin contamination ($\langle S^2 \rangle = 1.72$), and these energies are suspect quantitatively.

TABLE 1: Gibbs Free Energies (298 K) for All Intermediates and Transition States at the B3LYP/6-311+G//B3LYP/6-31G* Level**

	1	**TS 1−2a**	**2a**	**TS 2a-3**	**3**	**TS 2a-4**	**4**
phenyl	32.3	38.4	0.0	51.0	27.3	27.2	22.6
2-pyridinyl	28.5	34.7	0.0	37.6	30.5	30.8	25.3
3-pyridinyl	30.4	37.6	0.0	*a*	26.8	27.1	22.0
4-pyridinyl	29.9	36.1	0.0	37.7	31.0	30.3	26.0

	TS 2a-5a	**5a**	**TS 2a-2b**	**2b**	**TS 2b-5b**	**5b**
phenyl	46.2	44.8	*b*	*b*	*b*	*b*
2-pyridinyl	42.7	40.0	4.5	1.3	46.7	−33.7
3-pyridinyl	48.1	46.9	4.2	0.6	43.8	41.3
4-pyridinyl	47.3	45.5	*b*	*b*	*b*	*b*

[a] Despite numerous attempts, this stationary point could not be located at the B3LYP/6-31G* level. [b] Owing to symmetry, **2a** = **2b** and **5a** = **5b**.

C. Rearrangement of Pyridinylperoxy Radicals to Yield the Dioxiranylpyridinyl Radical Intermediates (2a → 4). The isomerization of an arylperoxy radical through the ring closure of the terminal oxygen to the proximal ring carbon (1,1-addition) forming a dioxiranyl intermediate (**4**, Figure 2) was first proposed by Carpenter[14] as a possible key step in the unimolecular decomposition of phenylperoxy radical. This proposal was further supported by B3LYP and CCSD(T) studies, which have shown that the dioxiranyl radical pathway for phenylperoxy radical is favored at temperatures ≤1250 K.[16] Therefore, it is not surprising that the dioxiranyl radical intermediates from the pyridinylperoxy radicals are the most stable at 298 K.

The rearrangement of pyridinylperoxy radical (**2**) to form the dioxiranyl radical (**4**) is an endoergic process owing to the loss of aromaticity in the pyridinyl ring, but some stability is gained through the delocalization of the electron throughout the ring. The order of stability for the dioxiranylpyridinyl radicals is 3- (+22.0 kcal/mol) > 2- (+25.3 kcal/mol) > 4- (+26.0 kcal/mol) and is related to the ability of each system to delocalize the electron as well as the electron-withdrawing nature of the ring nitrogen with respect to the position of the dioxiranyl functional group.

The free energies of activation at 298 K for forming the dioxiranyl radicals (**4**) are the lowest of any explored on these potential energy surfaces. $\Delta G^{\ddagger}$(298 K) is ∼30 kcal/mol for the formation of 2- and 4-dioxiranylpyridinyl radicals, while the barrier is only ∼27 kcal/mol for the 3-dioxiranylpyridinyl radical. Therefore, the rearrangement of the pyridinylperoxy radical (**2a**) to yield the corresponding dioxiranylpyridinyl radical (**4**) is the energetically most favorable pathway at 298 K, which is similar to the observations made for phenylperoxy radical.

D. Rearrangement of Pyridinylperoxy Radicals To Form a Dioxetanylpyridinyl Radical Intermediate (2a → 5a or 2a → 2b → 5b). The 1,2-addition of the terminal oxygen in the pyridinylperoxy radicals to a neighboring carbon or nitrogen

TABLE 2: Free Energies of Activation Leading from Arylperoxy Radicals as a Function of Temperature at the B3LYP/6-311+G//B3LYP/6-31G* Level**

	TS 1−2a	TS 2a-2b	TS 2a-3	TS 2a-4	TS 2a-5a	TS 2b-5b
			298 K			
phenyl	38.4	*a*	51.0	27.2	46.2	*a*
2-pyridinyl	34.7	4.5	37.6	30.8	42.7	46.7
3-pyridinyl	37.6	4.2	*b*	27.1	48.1	43.8
4-pyridinyl	36.1	*a*	37.7	30.3	47.3	*a*
			500 K			
phenyl	34.9	*a*	49.8	27.6	46.9	*a*
2-pyridinyl	31.0	5.2	36.3	31.1	43.4	47.0
3-pyridinyl	34.5	5.0	*b*	27.4	48.8	44.5
4-pyridinyl	32.4	*a*	37.1	30.5	48.0	*a*
			1000 K			
phenyl	26.6	*a*	46.8	28.6	49.0	*a*
2-pyridinyl	22.1	7.6	33.0	32.3	45.5	48.3
3-pyridinyl	27.3	7.4	*b*	28.4	50.9	46.8
4-pyridinyl	23.5	*a*	35.9	31.5	49.9	*a*
			1500 K			
phenyl	18.7	*a*	44.3	30.1	51.5	*a*
2-pyridinyl	13.6	10.4	30.1	33.9	48.1	50.0
3-pyridinyl	20.5	10.3	*b*	29.8	53.4	49.5
4-pyridinyl	15.0	*a*	35.0	32.7	52.2	*a*
			2000 K			
phenyl	11.0	*a*	42.0	31.8	54.2	*a*
2-pyridinyl	5.4	13.6	27.4	35.7	50.9	51.9
3-pyridinyl	13.9	13.6	*b*	31.5	56.2	52.5
4-pyridinyl	6.8	*a*	34.3	34.2	54.8	*a*

[a] Owing to symmetry, **2a** = **2b** and **5a** = **5b**. [b] Despite numerous attempts, this stationary point could not be located at the B3LYP/6-31G* level.

atom in the pyridine ring can occur either from the most stable conformation (**2a**) of the pyridinylperoxy radical or following the rotation (**2a** → **2b**) of the peroxy group (Figure 2). The barrier to rotation ($\Delta G^{\ddagger}$, 298 K) is ∼4 kcal/mol for both 2- and 3-pyridinylperoxy radicals, while the activation barrier for dioxetane formation (1,2-addition) ranges from 42.7 to 48.1 kcal/mol for the formation of all possible dioxetanylpyridinyl radicals.

Formation of the dioxetane ring is endoergic, with ΔG(298 K) ranging from +40.0 to +46.9 kcal/mol for all reactions explored except for the one resulting in the 2-pyridinyl-**5b** intermediate (Figure 2). The reaction, which yields 2-pyridinyl-**5b** from 2-pyridinyl-**2b**, is highly exoergic (−33.7 kcal/mol at 298 K). This 1,2-addition reaction is unique as the activation barrier is similar to the production of the other dioxetanes, but the product gains stability through the scission of the O−O bond. The B3LYP/6-31G* optimized geometry of this molecule suggests that the radical is localized on the O attached to the N since the N−O bond length is 1.270 Å, which is typical of an N−O single bond. (Such nitrosyl radicals are very stable and are often used as spin traps in EPR spectroscopy.[33])

The reaction mechanism and energetics for NO extrusion from 2-pyridinyl-**5b** (and related isomers) will be presented in a subsequent paper[34] and may proceed in a manner analogous to CO extrusion from the phenoxy radical as first proposed by Colussi et al.[4]

Although the dioxetanyl pathway possesses the largest activation barrier of any of the reactions studied here, it cannot be wholly discounted. In our previous study of the unimolecular decomposition of phenylperoxy radical, the dioxetanyl intermediate showed similar energetics (Table 1) but could readily break the O−O bond ($\Delta G^{\ddagger} = -0.3$ kcal/mol at 298 K) to form a very stable intermediate ($\Delta G = -18.0$ kcal/mol at 298 K).[16] This overall, exoergic process for O−O cleavage, analogous to the one-step reaction that yields 2-pyridinyl-**5b**, can be expected to occur with similar energetics for all of the dioxetanylpyridinyl radicals.

TABLE 3: Gibbs Free Energies (298−2000 K) for All Intermediates at the B3LYP/6-311+G//B3LYP/6-31G* Level**

	1	2a	2b	3	4	5a	5b
				298 K			
phenyl	32.3	0.0	*a*	27.3	22.6	44.8	*a*
2-pyridinyl	28.5	0.0	1.3	30.5	25.3	40.0	−33.7
3-pyridinyl	30.4	0.0	0.6	26.8	22.0	46.9	41.3
4-pyridinyl	29.9	0.0	*a*	31.0	26.0	45.5	*a*
3-pyridazinyl	27.1	0.0	1.1	25.3	25.9	39.6	−44.6
4-pyridazinyl	26.9	0.0	0.6	28.6	23.6	45.3	42.7
2-pyrimidinyl	28.4	0.0	*a*	34.2	28.1	−33.6	*a*
4-pyrimidinyl	26.8	0.0	1.2	34.6	29.3	40.4	−33.3
5-pyrimidinyl	28.9	0.0	*a*	29.4	21.7	43.2	*a*
pyrazinyl	26.2	0.0	0.8	28.5	22.8	35.4	−34.3
				500 K			
phenyl	24.9	0.0	*a*	20.6	22.8	45.2	*a*
2-pyridinyl	20.5	0.0	1.1	23.8	25.5	40.5	−33.6
3-pyridinyl	22.5	0.0	0.5	20.1	22.2	47.3	41.8
4-pyridinyl	22.0	0.0	*a*	24.3	26.1	45.9	*a*
3-pyridazinyl	19.2	0.0	0.4	18.4	25.8	40.1	−44.4
4-pyridazinyl	19.1	0.0	0.5	21.8	23.7	45.5	43.1
2-pyrimidinyl	20.6	0.0	*a*	27.5	28.4	−33.3	*a*
4-pyrimidinyl	18.8	0.0	1.0	27.8	29.4	40.8	−33.1
5-pyrimidinyl	21.1	0.0	*a*	23.1	21.8	43.8	*a*
pyrazinyl	18.3	0.0	0.6	21.7	22.9	36.0	−34.0
				1000 K			
phenyl	7.1	0.0	*a*	3.9	22.9	46.0	*a*
2-pyridinyl	1.9	0.0	0.5	6.8	25.5	41.4	−33.2
3-pyridinyl	4.1	0.0	0.4	3.3	22.1	48.2	42.9
4-pyridinyl	3.5	0.0	*a*	7.5	26.1	46.5	*a*
3-pyridazinyl	0.5	0.0	−1.5	1.1	25.3	41.1	−43.9
4-pyridazinyl	0.6	0.0	0.4	4.7	23.5	46.0	43.9
2-pyrimidinyl	2.4	0.0	*a*	10.7	28.9	−32.9	*a*
4-pyrimidinyl	0.2	0.0	0.5	10.7	29.2	41.7	−32.9
5-pyrimidinyl	3.0	0.0	*a*	7.1	21.8	45.2	*a*
pyrazinyl	−0.1	0.0	0.0	4.7	22.9	37.4	−33.5
				1500 K			
phenyl	−10.1	0.0	*a*	−12.7	22.8	46.6	*a*
2-pyridinyl	−16.1	0.0	−0.1	−10.1	25.5	42.2	−32.9
3-pyridinyl	−13.7	0.0	0.2	−13.4	21.9	48.9	43.9
4-pyridinyl	−14.4	0.0	*a*	−9.3	25.8	46.9	*a*
3-pyridazinyl	−17.6	0.0	−3.5	−16.2	24.6	42.0	−43.3
4-pyridazinyl	−17.2	0.0	0.3	−12.3	23.1	46.3	44.6
2-pyrimidinyl	−15.2	0.0	*a*	−6.1	29.2	−32.5	*a*
4-pyrimidinyl	−17.9	0.0	−0.1	−6.5	28.9	42.4	−32.7
5-pyrimidinyl	−14.5	0.0	*a*	−8.8	21.6	46.5	*a*
pyrazinyl	−17.8	0.0	−0.5	−12.3	22.7	38.8	−32.9
				2000 K			
phenyl	−26.9	0.0	*a*	−29.3	22.7	47.2	*a*
2-pyridinyl	−33.6	0.0	−0.7	−27.0	25.3	43.0	−32.6
3-pyridinyl	−31.1	0.0	0.0	−30.1	21.6	49.6	44.9
4-pyridinyl	−31.9	0.0	*a*	−26.1	25.5	47.3	*a*
3-pyridazinyl	−35.2	0.0	−5.4	−33.3	23.9	42.9	−42.8
4-pyridazinyl	−34.5	0.0	0.2	−29.3	22.6	46.6	45.2
2-pyrimidinyl	−32.3	0.0	*a*	−22.8	29.4	−32.0	*a*
4-pyrimidinyl	−35.4	0.0	−0.6	−23.5	28.6	43.0	−32.4
5-pyrimidinyl	−31.6	0.0	*a*	−24.7	21.3	47.7	*a*
pyrazinyl	−35.1	0.0	−1.0	−29.3	22.4	40.1	−32.4

[a] Owing to symmetry, **2a** = **2b** and **5a** = **5b**.

E. Comparison of the Reaction Pathways as a Function of Temperature. Several general trends are observed when the Gibbs free energies and activation barriers are compared at temperatures ranging from 500 to 2000 K (Tables 2 and 3). On the basis of free energies of activation, the most accessible pathway for the pyridinylperoxy radicals at temperatures ≤500 K is the production of the dioxiranyl intermediate. At temperatures ≥1000 K, the loss of O_2 from the pyridinylperoxy radical to regenerate the pyridinyl radical has the lowest activation

TABLE 4: Relative Energies (kcal/mol) at Different Theoretical Levels for a Few Important Intermediates and Transition States for 2-Pyridinyl Radical[a]

	2a	TS 2a-2b	TS 1−2	TS 2a-3	TS 2a-4	TS 2a-5a	TS 2b-5b
UMP2/6-31G**	0.0	3.1	61.7	64.0	54.5	70.6	105.6
UMP3/6-31G**	0.0	2.8	56.1	43.2	45.9	62.6	91.9
UMP4(SDQ)/6-31G**	0.0	3.2	51.4	40.6	41.9	57.3	86.8
UCCSD/6-31G**	0.0	3.6	43.0	31.7	33.3	46.6	60.2[b]
UCCSD(T)/6-31G**	0.0	4.0	44.3	36.9	32.5	44.7	*b*
UB3LYP/6-311+G**	0.0	4.4	41.8	42.0	32.1	43.4	47.6
UB3LYP/6-31G*	0.0	5.1	44.5	46.1	31.7	43.0	49.1
UB3LYP/6-311+G** $\langle S^2 \rangle$	0.76	0.75	1.76	1.79	0.78	0.77	0.76
UCCSD(T)/6-31G** $\langle S^2 \rangle$	0.77	0.76	2.40	2.40	1.43	1.43	1.90

[a] The B3LYP/6-31G* geometry was used in each case, and the energies are at the bottom-of-the-well. [b] The CCSD equations could not be converged to the necessary accuracy ($<10^{-7}$ au) by Gaussian 98 in order to complete the UCCSD(T) calculation. The corresponding CCSD energy for **TS 2b-5b** reflects a 10^{-5} au convergence.

barrier. This feature, especially when coupled with the knowledge that the reaction of pyridinyl radical with O_2 at temperatures greater than 1000 K is endoergic, decreases the likelihood of the pyridinylperoxy radical as an intermediate at high temperatures. Furthermore, at 2000 K, the transition state for loss of O_2 has a lower free energy of activation than rotation of the peroxy functional group on the pyridinylperoxy radicals.

Another distinct trend is the similarity of the 3-pyridinyl radical with O_2 potential energy surface (PES) with that of the phenyl radical with O_2. Notably, the Gibbs free energy of the 3-pyridinyloxy or phenoxy radical (**3**) with O atom at infinite separation is more stable than the 3-pyridinyl or phenyl radical with O_2 at temperatures <1500 K. In stark contrast, 2- and 4-pyridinyl radical with O_2 complexes are more energetically favored than their pyridinyloxy radical counterpart at all temperatures. This is an important trend since the C−H BDEs in pyridine, based on either calculated[12] or experimental[10] values, is 2- < 4- ≈ 3-pyridinyl radical. As the C−H BDE to generate the 2-pyridinyl radical is ∼5 kcal/mol more favored than at the other positions,[10,12] the trends of the 2-pyridinylperoxy radical are of increased importance. The greatest contrast in the PES of 2-pyridinylperoxy radical versus that of 3- or 4-pyridinylperoxy radicals is that at temperatures as low as 500 K, the free energy of activation for the loss of O_2 (31.0 kcal/mol) is equivalent to the barrier for dioxiranyl formation (31.1 kcal/mol), while the overall loss of O_2 is less endoergic.

F. Comparison of Theoretical Levels. We have also calculated single-point energies at the UCCSD(T)/6-31G** level for 2-pyridinylperoxy radical and its transition states to evaluate the quantitative accuracy of the B3LYP energies. These relative energies (at the bottom of the well) are provided in Table 4. The UCCSD(T) energies are in good qualitative and quantitative agreement with the B3LYP results, except for structures **TS 2a-3** and **TS 2b-5b**.

The **TS 2a-3** calculations at both the B3LYP and UCCSD(T) levels experience significant spin contamination problems ($\langle S^2 \rangle = 1.79$ and 2.40, respectively), and these energies are suspect quantitatively. For **TS 2b-5b**, the B3LYP calculation had negligible spin contamination ($\langle S^2 \rangle = 0.76$), while the UHF/6-31G** wave function had excessive spin contamination ($\langle S^2 \rangle = 1.90$) and also failed to converge the coupled-cluster equations for the UCCSD calculation.

IV. Other Azabenzenes: Pyridazine, Pyrimidine, and Pyrazine

We have also examined the reactivity (by calculating relevant intermediates) of three diazines: pyridazine (Figure 4), pyrimidine (Figure 5), and pyrazine (Figure 6). In observing trends for these diazines, the best indicator for reactivity of the peroxy radicals are the C−H BDEs from the parent aromatic compound.

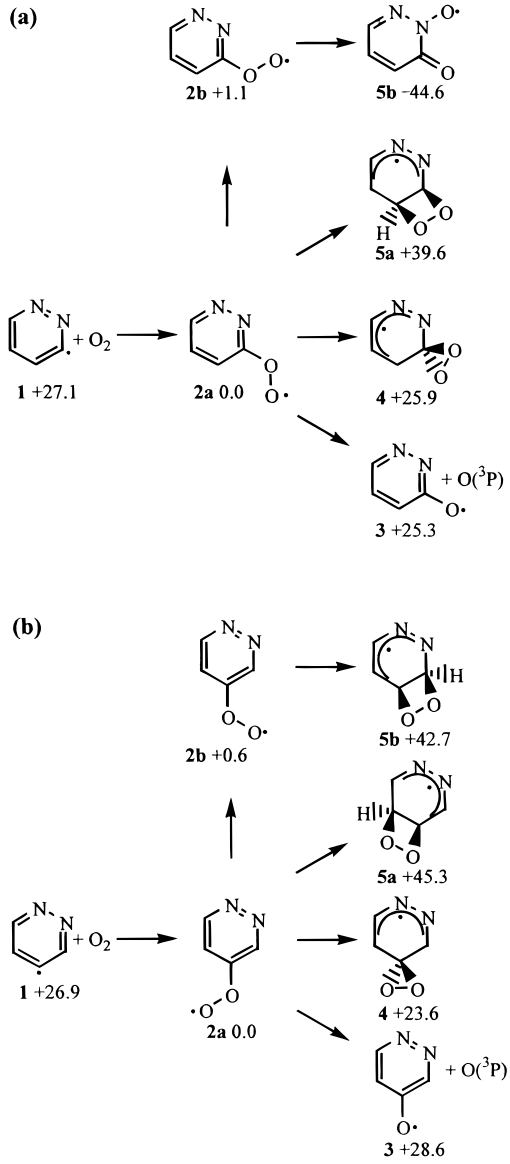

Figure 4. Mechanisms of the (a) 3-pyridazinyl + O_2 and (b) 4-pyridazinyl + O_2 reactions showing Gibbs free energies of each intermediate at 298 K (relative to the corresponding **2a**) at the B3LYP/6-311+G**//B3LYP/6-31G* level.

As noted in previous computational[12,35] and experimental studies,[9,10] H-atom abstraction is favored at positions ortho to the ring nitrogen followed by a slight preference for para over meta (Figure 7). When the C−H BDE is low for generating the parent radical prior to O_2 addition, the relative free energies for the decomposition or rearrangement of the peroxy radical

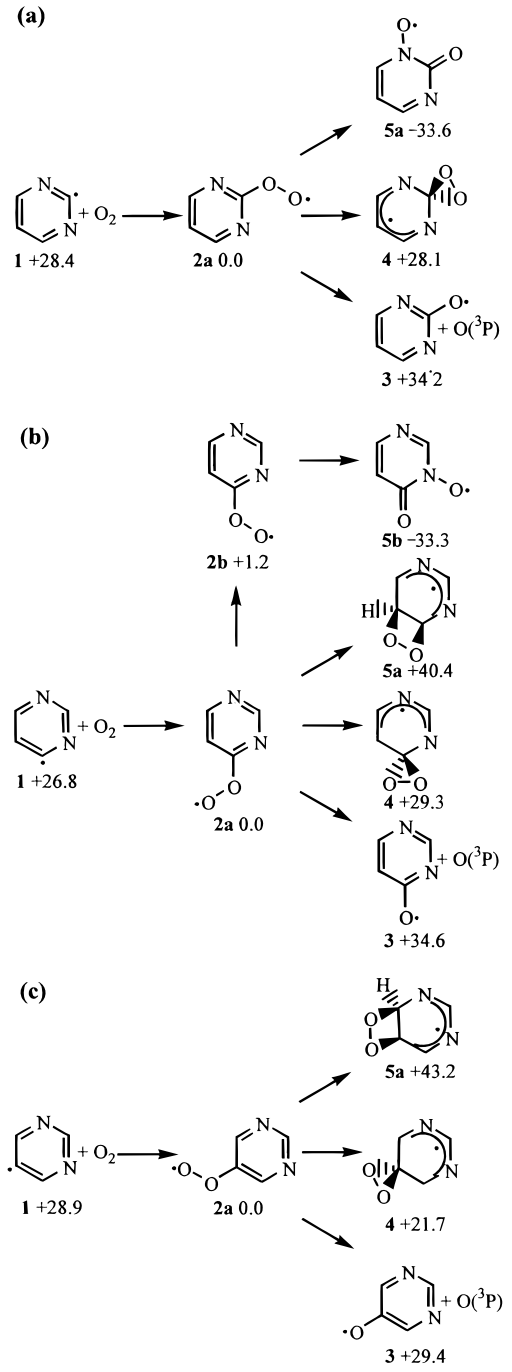

Figure 5. Mechanisms of the (a) 2-pyrimidinyl + O_2, (b) 4-pyrimidinyl + O_2, and (c) 5-pyrimidinyl + O_2 reactions showing Gibbs free energies of each intermediate at 298 K (relative to the corresponding **2a**) at the B3LYP/6-311+G**//B3LYP/6-31G* level.

are similar to those calculated for the 2-pyridinylperoxy radical. On the contrary, the higher the C−H BDE, the more closely the system resembles that of phenylperoxy radical.

The first significant trend is that the loss of O_2 from the parent arylperoxy radical is less endoergic than the loss of O atom leading to the aryloxy radical at all temperatures studied for most of the azabenzenes (Figure 7 and Table 3). Exceptions to this trend are the 3-pyridazinylperoxy and 3-pyridinylperoxy radicals. The reasons for the inverse relationship for 3-pyridinylperoxy radical were discussed above and are not the same causes for the unique stability of 3-pyridazinyloxy radical. Calculations for the 3-pyridazinyloxy radical reveal that the most stable electronic state is $^2A'$, i.e.; the unpaired electron is in the

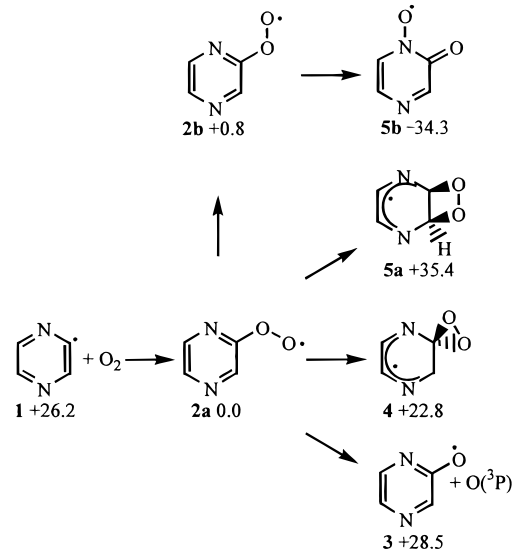

Figure 6. Mechanism of the pyrazinyl + O_2 reaction showing Gibbs free energies of each intermediate at 298 K (relative to the corresponding **2a**) at the B3LYP/6-311+G**//B3LYP/6-31G* level.

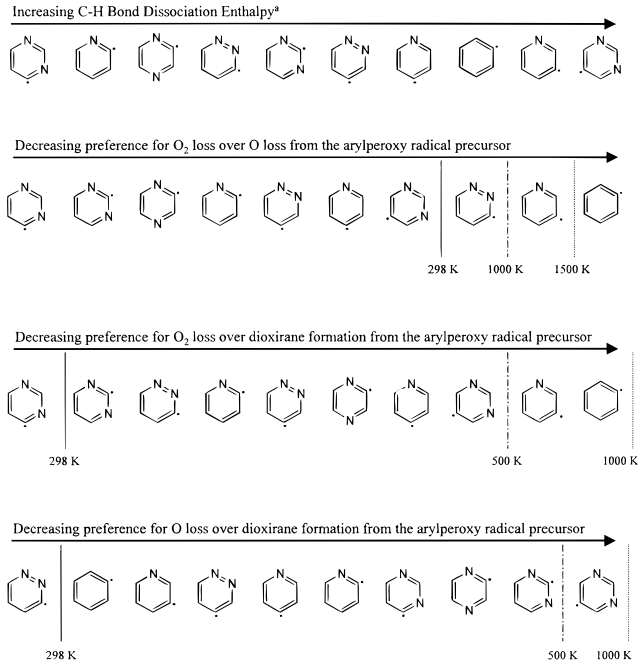

Figure 7. Observed trends of arylperoxy radical decomposition compared to the related C−H BDE as a function of temperature. Vertical lines represent the temperature of the crossover point for preference of the first pathway over the second. [a] See ref 12.

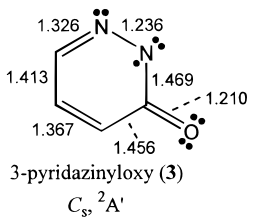

Figure 8. Molecular structure and critical bond lengths (Å) of 3-pyridazinyloxy at the B3LYP/6-31G* level.

σ system (Figure 8). This is in contrast to all of the other aryloxy radicals, for which the $^2A''$ (π) electronic state is more stable than the $^2A'(\sigma)$ state. Therefore, in the 3-pyridazinyloxy radical, the unpaired electron is centered on the proximal ring N to the carbonyl group in a σ orbital so as to maintain the ring's

aromatic character (6π e^-) relative to its 3-pyridazinylperoxy radical precursor.

Another predominant trend is that the formation of the dioxiranyl radical intermediate is less endoergic than either O_2 loss or O atom loss at 298 K. The only exceptions to this trend are O atom loss from the 3-pyridazinylperoxy radical for reasons discussed previously and O_2 loss from the 4-pyrimidinylperoxy radical. By 500 K, dioxiranyl radical formation is less favorable than O_2 loss or O atom loss in every azabenzene except for O_2 loss from the 3-pyridinylperoxy radical and O atom loss from 5-pyrimidinylperoxy radical. These observations are depicted in Figure 7 with vertical lines showing the crossover temperature for the preference of one pathway over the other. The energy difference between the dioxiranyl radicals and the aryloxy radicals with O atom or the aryl radical with O_2 is directly correlated to the respective C−H BDEs of the parent arene (Table 3 and Figure 7).

The dioxetanyl radical intermediates are generally the least stable of all studied and are between 11 and 22 kcal/mol less stable than their dioxiranyl radical counterparts. Exceptions to this trend are the 3-pyridazinyl-**5b**, 2-pyrimidinyl-**5a**, 4-pyrimidinyl-**5b**, and pyrazinyl-**5b** intermediates, which are all stable nitrosyl radicals (Figures 4−6). These four molecules possess increased stability over their peroxy radical counterparts, ranging from −33.3 to −44.6 kcal/mol (ΔG, 298 K). On the basis of our calculations for the pyridinyl radical system, the transition states connecting the arylperoxy radicals to these four nitrosyl radicals would have an estimated free energy of activation of ≥45 kcal/mol. Thus, despite the very stable products, the activation barrier is still very substantial and not competitive to other pathways for decomposition.

V. Conclusions

Detailed potential energy surfaces for the reaction of pyridinyl radicals with O_2 and subsequent reactions have been presented. Comparisons between the reactivity of pyridinylperoxy and diazaarylperoxy radicals with the phenylperoxy radical have been addressed. Oxidative mechanisms have been explored through a range of temperatures relevant to atmospheric and combustion processes.

Contrary to phenylperoxy radical decomposition, O_2 dissociation from the arylperoxy radical is preferred rather than the loss of O atom to generate the corresponding aryloxy radical. Formation of dioxiranyl radical intermediates is the most accessible pathway from the peroxy precursor at temperatures ≤500 K. Dioxetanyl intermediates are less favored energetically but generate stable nitrosyl radicals that may provide a route to NO_x generation.

Acknowledgment. We gratefully acknowledge the U.S. Department of Energy (Grant DE-FG22-96PC96249), the Ohio Supercomputer Center, and the U.S. Army for support of this research. We also thank Paul R. Rablen (Swarthmore College) for providing his Thermo94 program.

Supporting Information Available: Energies, enthalpies, free energies as a function of temperature, and moments of inertia for all intermediates and transition states for the reaction of each aryl radical with O_2. Cartesian coordinates and harmonic frequencies for all intermediates and transition states for each aryl radical with O_2. This material is available free of charge via the Internet at http://pubs.acs.org.

References and Notes

(1) (a) Smith, K. L.; Smoot, L. D.; Fletcher, T. H.; Pugmire, R. J. *The Structure and Reaction Processes of Coal*; Plenum Press: New York, 1994. (b) Meyers, R. A. *Coal Structure*; Academic Press: New York, 1982.

(2) Brezinsky, K. *Prog. Energy Combust. Sci.* **1986**, *12*, 1−24.

(3) Bittker, D. A. *Combust. Sci. Technol*. **1991**, *79*, 49−72.

(4) Colussi, A. J.; Zabel, F.; Benson, S. W. *Int. J. Chem. Kinet*. **1977**, *9*, 161−178.

(5) Zhang, H.-Y.; McKinnon, J. T. *Combust. Sci. Technol*. **1995**, *107*, 261−300.

(6) Chai, Y.; Pfefferle, L. D. *Fuel* **1998**, *77*, 313−320.

(7) (a) Nimmo, W.; Richardson, J.; Hampartsoumian, E. *J. Inst. Energy* **1995**, *68*, 170−177. (b) Williams, A.; Pourkashanian, M.; Jones, J. M.; Rowlands, L. *J. Inst. Energy* **1997**, *70*, 102−113.

(8) Mackie, J. C.; Colket, M. B., III.; Nelson, P. F. *J. Phys. Chem.* **1990**, *94*, 4099−4106.

(9) Doughty, A.; Mackie, J. C. *J. Chem. Soc., Faraday Trans.* **1994**, *90*, 541−548.

(10) Kiefer, J. H.; Zhang, Q.; Kern, R. D.; Yao, J.; Jursic, B. *J. Phys. Chem. A* **1997**, *101*, 7061−7073.

(11) Morris, V. R.; Bhatia, S. C.; Stelson, A. W.; Hall, J. H. *Energy Fuels* **1991**, *5*, 126−133.

(12) See Barckholtz, C.; Barckholtz, T. A.; Hadad, C. M. *J. Am. Chem. Soc.* **1999**, *121*, 491−500 and the references therein.

(13) Yu, T.; Lin, M. C. *J. Am. Chem. Soc*. **1994**, *116*, 9571−9576.

(14) Carpenter, B. K. *J. Am. Chem. Soc*. **1993**, *113*, 9806−9807.

(15) Barckholtz, C.; Fadden, M. J.; Hadad, C. M. *J. Phys. Chem. A* **1999**, *103*, 8108−8117.

(16) Fadden, M. J.; Barckholtz, C.; Hadad, C. M. *J. Phys. Chem. A* **2000**, *104*, 3004−3011.

(17) (a) Labanowski, J. W.; Andzelm, J. *Density Functional Methods in Chemistry*; Springer: New York, 1991. (b) Parr, R. G.; Yang, W. *Density Functional Theory in Atoms and Molecules*; Oxford University Press: New York, 1989.

(18) (a) Cioslowski, J.; Liu, G.; Martinov, M.; Piskorz, P.; Moncrieff, D. *J. Am. Chem. Soc.* **1996**, *118*, 5261−5264. (b) Cioslowski, J.; Liu, G.; Moncrieff, D. *J. Org. Chem.* **1996**, *61*, 4111−4114.

(19) Frisch, M. J.; Trucks, G. W.; Schlegel, H. B.; Gill, P. M. W.; Johnson, B. G.; Robb, M. A.; Cheeseman, J. R.; Keith, T.; Petersson, G. A.; Montgomery, J. A.; Raghavachari, K.; Al-Laham, M. A.; Zakrzewski, V. G.; Ortiz, J. V.; Foresman, J. B.; Peng, C. Y.; Ayala, P. Y.; Chen, W.; Wong, M. W.; Andres, J. L.; Replogle, E. S.; Gomperts, R.; Martin, R. L.; Fox, D. J.; Binkley, J. S.; Defrees, D. J.; Baker, J.; Stewart, J. J. P.; Head-Gordon, M.; Gonzalez, C.; Pople, J. A. Gaussian 94, Revision D.3; Gaussian, Inc.; Pittsburgh, PA, 1995.

(20) Frisch, M. J.; Trucks, G. W.; Schlegel, H. B.; Scuseria, G. E.; Robb, M. A.; Cheeseman, J. R.; Zakrzewski, V. G.; Montgomery, J. A., Jr.; Stratmann, R. E.; Burant, J. C.; Dapprich, S.; Millam, J. M.; Daniels, A. D.; Kudin, K. N.; Strain, M. C.; Farkas, O.; Tomasi, J.; Barone, V.; Cossi, M.; Cammi, R.; Mennucci, B.; Pomelli, C.; Adamo, C.; Clifford, S.; Ochterski, J.; Petersson, G. A.; Ayala, P. Y.; Cui, Q.; Morokuma, K.; Malick, D. K.; Rabuck, A. D.; Raghavachari, K.; Foresman, J. B.; Cioslowski, J.; Ortiz, J. V.; Stefanov, B. B.; Liu, G.; Liashenko, A.; Piskorz, P.; Komaromi, I.; Gomperts, R.; Martin, R. L.; Fox, D. J.; Keith, T.; Al-Laham, M. A.; Peng, C. Y.; Nanayakkara, A.; Gonzalez, C.; Challacombe, M.; Gill, P. M. W.; Johnson, B.; Chen, W.; Wong, M. W.; Andres, J. L.; Gonzalez, C.; Head-Gordon, M.; Replogle, E. S.; Pople, J. A. Gaussian 98, Revision A.7; Gaussian, Inc.; Pittsburgh, PA, 1998.

(21) Becke, A. D. *Phys. Rev. A* **1988**, *38*, 3098−3100.

(22) Lee, C.; Yang, W.; Parr, R. G. *Phys. Rev. B* **1988**, *37*, 785−789.

(23) Becke, A. D. *J. Chem. Phys.* **1993**, *98*, 1372.

(24) Hehre, W. J.; Radom, L.; Schleyer, P. v. R.; Pople, J. A. *Ab Initio Molecular Orbital Theory*; John Wiley & Sons: New York, 1986.

(25) Bauschlicher, C. W., Jr.; Langhoff, S. R. *Mol. Phys.* **1999**, *96*, 471.

(26) Stanton, J. F.; Gauss, J.; Watts, J. D.; Lauderdale, W. J.; Bartlett, R. J. *Int. J. Quantum Chem.* **1992**, *S26*, 879.

(27) Scott, A. P.; Radom, L. *J. Phys. Chem*. **1996**, *100*, 16502−16513.

(28) Rablen, P. R. Thermo94; Yale University, 1994.

(29) Chase, M. W., Jr. *NIST-JANAF Thermochemical Tables*; American Chemical Society: Washington, D.C.; American Institute of Physics for the National Institute of Standards and Technology, New York, 1998.

(30) Alfassi, Z. B.; Khailkin, G. I.; Neta, P. *J. Phys. Chem.* **1995**, *99*, 4544−4548.

(31) Das, T. N.; Neta, P. *J. Phys. Chem. A* **1998**, *102*, 7081−7085.

(32) As cited in: Knyazev, V. D.; Slagle, I. R. *J. Phys. Chem.* **1995**, *99*, 2247−2249.

(33) (a) Janzen, E. G. *Acc. Chem. Res.* **1971**, *4*, 31. (b) Perkins, M. J. *Adv. Phys. Org. Chem.* **1980**, *17*, 1. (c) Janzen, E. G.; Evans, C. A.; Davis, E. R. In *Organic Free Radicals*; ACS Symposium Series 69; American Chemical Society: Washington, D.C., 1978; p 433.

(34) Fadden, M. J.; Hadad, C. M. Manuscript in preparation.

(35) Jones, J.; Backsay, G. B.; Mackie, J. C.; Doughty, A. *J. Chem. Soc., Faraday Trans.* **1995**, *91*, 1587−1592.